

Nanoparticle Probes

DOI: 10.1002/anie.200603052

Dual-Mode Nanoparticle Probes for High-Performance Magnetic Resonance and Fluorescence Imaging of Neuroblastoma**

Jae-Hyun Lee, Young-wook Jun, Soo-In Yeon, Jeon-Soo Shin,* and Jinwoo Cheon*

Inorganic nanoparticles are emerging as potential probes in next-generation biomedical applications.^[1] Their enhanced

[*] S.-I. Yeon, Prof. J.-S. Shin
Department of Microbiology
College of Medicine
Yonsei University
Seoul 120-752 (Korea)
E-mail: jsshin6203@yumc.yonsei.ac.kr
J.-H. Lee, Dr. Y.-w. Jun, Prof. J. Cheon
Department of Chemistry
Yonsei University
Seoul 120-749 (Korea)
Fax: (+82) 2-364-7050
E-mail: jcheon@yonsei.ac.kr

[**] We thank Dr. H. S. Kwon and J.-M. Oh for TEM analyses (KBSI-Chuncheon), and Prof. J.-S. Suh, Prof. Y.-M. Huh (Yonsei), Dr. O. H. Han, and S. H. Kim for MRI (KBSI-Daegu). This work was supported in part by the National Research Laboratory (M10600000255), R&D Program for Cancer Control of Ministry of Health & Welfare (0320250-2), NCRC (R15-2004-024-00000-0), NCI Center for Nanotechnology Excellence, IT Leading R&D Support Project, AOARD-AFOSR, 2nd stage BK21 for Medical Science and Chemistry, and Korea Health 21 R&D Project of Ministry of Health & Welfare (A050260).

Supporting information for this article is available on the WWW under <http://www.angewandte.org> or from the author.

properties arising from nanoscale effects and their comparable size to biofunctional molecules have allowed for ultra-sensitive detection of biomolecular targets.^[1-3] Of the various nanoparticles, quantum dots and fluorescent-dye-doped silica nanoparticles are representative examples of optical nanoprobe systems.^[2] Dye-doped silica nanoparticles have several advantages for optical imaging: 1) high photostability arising from the stabilization of dye molecules in a protective silica matrix,^[2a] 2) amplification of the fluorescent signal owing to high dye-incorporation capabilities of silica nanoparticles,^[2b,c] and 3) the silica is known to be relatively biocompatible and less toxic.^[2d]

On the other hand, magnetic nanoparticles exhibit a unique magnetic-resonance (MR) contrast enhancement effect that enables noninvasive MR imaging of cell trafficking, gene expression, and cancer.^[3] However, retrieving detailed biological information on a subcellular level is difficult owing to limited resolution and low sensitivity of the MRI technique. Until now, most previous studies that utilized optical and/or magnetic nanoparticle probes have been focused on monofunctional probes, except for a few primitive dual probes such as the single magnetic nanoparticle that was directly linked to organic dyes.^[4]

Our strategy for the development of the next generation of nanoprobe has been to fuse multiple fluorescent dyes and multiple magnetic nanoparticles into a single nanoprobe that provides superior fluorescence and MR imaging capabilities through the synergistic enhancement of its respective components. Specifically, we have fabricated new “core–satellite” structured dual functional nanoparticles comprised of a dye-doped silica “core” and multiple “satellites” of magnetic nanoparticles. We further demonstrate their utilization as simultaneous optical and MR imaging of neuroblastoma cells expressing polysialic acids (PSAs). Detection of PSA is important as it is not only an important carbohydrate associated with neural pathways, such as synaptic plasticity, learning and memory, and cell-to-cell interaction,^[5] but it is also a marker of neuroblastoma, lung carcinoma, and Wilms’ tumors.^[6]

Rhodamine-dye-doped silica (DySiO₂) nanoparticles with surface amine groups were synthesized by a modified literature method.^[2e] The obtained nanoparticles have a homogeneous size of 30 nm (Figure 1 b). High-quality water-soluble iron oxide (Fe₃O₄, abbreviated as WSIO) nanoparticles were synthesized following a method previously reported by us.^[7] The WSIO nanoparticles are 9 nm in diameter with high monodispersity ($\sigma \approx 5\%$) and coated with 2,3-dimercaptosuccinic acid (DMSA; Figure 1 c).

Our core–satellite nanoparticles were fabricated through the conjugation of these DySiO₂ nanoparticles with WSIO by using sulfosuccinimidyl-(4-N-maleimidomethyl)cyclohexane-1-carboxylate (sulfo-SMCC, Pierce) cross-linkers (Figure 1 a). First, the amine groups of the DySiO₂ nanoparticle were modified with maleimide groups by reacting them with sulfo-SMCC cross-linkers. The reactions between the maleimide groups of the silica nanoparticle and the thiol groups of WSIO nanoparticles subsequently yielded hybrid nanoparticles ((DySiO₂–(Fe₃O₄)_n, $n = 10 \pm 2$) of a dye-doped silica core and iron oxide satellites.

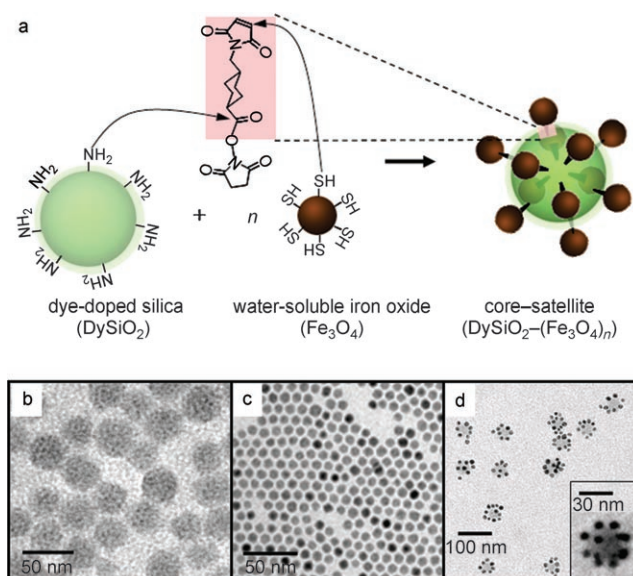


Figure 1. a) Schematic diagram for the synthesis of core-satellite DySiO₂-(Fe₃O₄)_n nanoparticles. b–d) TEM images of b) rhodamine-doped silica (DySiO₂), c) iron oxide (Fe₃O₄), and d) core-satellite DySiO₂-(Fe₃O₄)_n nanoparticles.

Figure 1d shows a transmission electron microscopy (TEM) image of obtained DySiO₂-(Fe₃O₄)_n nanoparticles. The hybrid nanoparticles are composed of a silica core linked by roughly 10 WSIO nanoparticle satellites. Both nanoparticle components retained their initial sizes, and the overall size of the hybrid nanoparticles is approximately 45 nm. Hybrid nanoparticles are stable in aqueous media and phosphate buffer solution.

We first examined the MR contrast effect of DySiO₂-(Fe₃O₄)_n nanoparticles in comparison with that of free WSIO nanoparticles with the same iron concentration. In the spin-spin relaxation time (T₂) weighted spin echo MRI at 9.4 T, the free WSIO nanoparticles show weak MR contrast with a T₂ relaxivity coefficient (*r*₂) of 116 mm⁻¹s⁻¹ (Figure 2a,c). In contrast, the DySiO₂-(Fe₃O₄)_n nanoparticles provide a

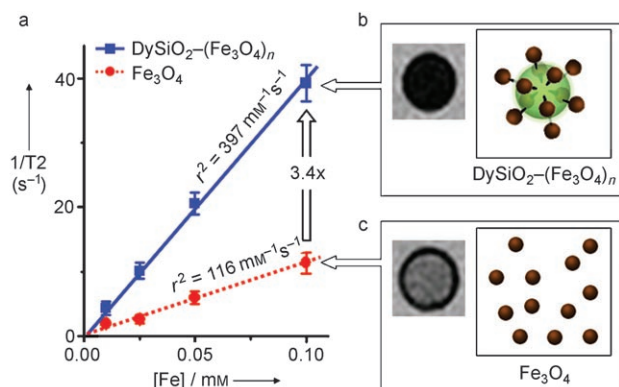


Figure 2. Synergistic MR enhancement effect of DySiO₂-(Fe₃O₄)_n. T₂ relaxivity coefficients (*r*₂; a) and T₂-weighted MR images (b,c) of DySiO₂-(Fe₃O₄)_n nanoparticles (b) and free Fe₃O₄ nanoparticles (c). A 3.4-fold increase in *r*₂ is observed for DySiO₂-(Fe₃O₄)_n nanoparticles.

remarkably dark MR contrast of an approximate 3.4-fold increased T₂ relaxivity coefficient of 397 mm⁻¹s⁻¹ (Figure 2a,b). Such a significant improvement in the MR signal arises from the synergistic magnetism of multiple Fe₃O₄ satellites surrounding a core silica nanoparticle.^[8] Furthermore, our DySiO₂-(Fe₃O₄)_n nanoparticles exhibit enhanced fluorescence behavior at λ ≈ 580 nm of rhodamine dye molecules with approximately 1.7-times more intense emission, compared with that of directly conjugated rhodamine-Fe₃O₄ nanoparticles (see the Supporting Information).^[2a]

As a case study for their utilization in dual-mode imaging of neuroblastoma model cells expressing PSAs, we conjugated DySiO₂-(Fe₃O₄)_n hybrid nanoparticles with HmenB1 antibodies through sulfo-SMCC conjugation. HmenB1 antibody has been known to specifically target cells with PSAs.^[9] The nanoparticle-HmenB1 conjugates were then tested on two different cell lines: target CHP-134 cells with over-expression of PSA and control HEK293T cells without PSA expression. In the T₂*-weighted gradient echo images at 9.4 T, a high MR contrast effect is seen for the nanoparticle-HmenB1 conjugate treated CHP-134 cells (Figure 3a),

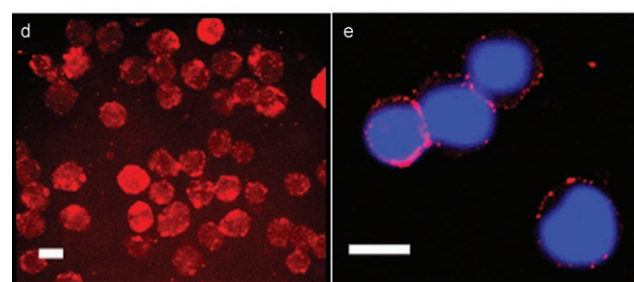
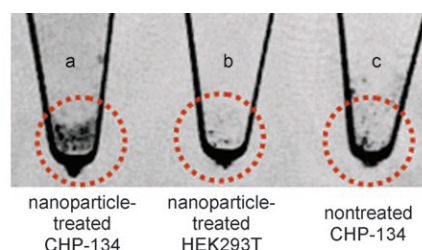


Figure 3. Dual-mode detection of PSAs. T₂*-weighted MR images of CHP-134 cells treated with the DySiO₂-(Fe₃O₄)_n-HmenB1 conjugate (a), HEK293T cells treated with the DySiO₂-(Fe₃O₄)_n-HmenB1 conjugate (b), and nontreated CHP-134 cells (c). d) Fluorescence and e) confocal microscopy images of the same sample used in (a). Cell nuclei were stained a blue color with DAPI for confocal imaging. Scale bars: 10 μm.

whereas no MR contrast is observed from the nanoparticle-HmenB1 conjugate treated HEK293T cells (Figure 3b) and nontreated CHP-134 cells (Figure 3c). Fluorescence imaging of these cells shows consistent results. Strong red fluorescence is observed from the DySiO₂-(Fe₃O₄)_n nanoparticle-HmenB1 conjugate treated CHP-134 cells (Figure 3d), whereas no fluorescence activity is observed from the control HEK293T cells. Confocal microscope imaging provides spatial distribution of PSA expressions in which red fluorescence is only detected in the membrane regions of the CHP-134 cells

(Figure 3e). PSAs are expressed on the neural cell adhesion molecules (NCAMs) of the cell membrane, which is consistent with our observation.^[5] As it is not possible to have such detailed cellular information from the MRI results, it is noteworthy that dual-mode imaging is clearly advantageous to obtain both macroscopic and detailed subcellular information of biological events.

In summary, we have demonstrated the realization of high performance “core–satellite” structured nanoparticles with a synergistic MR contrast enhancement effect and good fluorescent properties. Subsequently, such nanoparticles were confirmed as excellent dual-imaging probes for the detection of PSAs expressed on various cell lines. The concept of multifunctional core–satellite hybrid nanoparticles can serve as a platform technology for the next-generation probes in the detection and imaging of biological targets.

Experimental Section

Synthesis of DySiO₂–(Fe₃O₄)_n nanoparticles: Dye-doped silica (DySiO₂) and 9-nm water-soluble iron oxide (Fe₃O₄, WSIO) nanoparticles were synthesized by a literature method.^[2c,4a] Our hybrid nanoparticles were fabricated through conjugation of these dye-doped silica nanoparticles with WSIO by using sulfo-SMCC (Pierce) cross-linkers. In a typical experiment, DySiO₂ nanoparticles were dissolved in 10 mM phosphate buffer solution (0.1 mL) with a final concentration of 5 mg mL⁻¹. The nanoparticle surface amine was modified with a maleimide group by adding sulfo-SMCC cross-linker molecules (30 μg). After 30 min, excess cross-linkers were removed by passing them through a desalting column and a 10 mg mL⁻¹ WSIO nanoparticle solution (50 μL) was added to the maleimide-modified silica nanoparticle solution. Unreacted WSIO nanoparticles were removed by passing them through Sephadex G-25 column (Amersham Biosciences). The formation of DySiO₂–(Fe₃O₄)_n nanoparticles was confirmed by gel electrophoretic analysis. A new band with delayed migration appears in both optical and fluorescence images when compared to those of WSIO and DySiO₂ nanoparticles (see the Supporting Information).

Iron oxide concentration determination: The iron oxide nanoparticle concentration was determined by repetitive measurement (*n* = 4) of Fe ion concentration through inductively coupled plasma atomic emission spectroscopy (ICP-AES) measurement after dissolving the nanoparticles in 1M sulfuric acid solution. The standard deviation is about 0.5%.

Conjugation of DySiO₂–(Fe₃O₄)_n nanoparticles with HmenB1 antibody: HmenB1 antibody (2 mg) was dissolved in 10 mM phosphate buffer solution (0.1 mL; pH 7.2) and sulfo-SMCC (30 μg) was added to the above solution. After 15 min, the maleimide-activated HmenB1 antibody was purified by applying the reaction mixture to a Sephadex G-25 (Aldrich) desalting column. Collected fractions (≈200 μL) containing maleimide-activated HmenB1 antibody were immediately mixed with a 2 mg Fe/mL DySiO₂–(Fe₃O₄)_n solution (100 μL) and reacted for 8 h at 4°C. DySiO₂–(Fe₃O₄)_n–HmenB1 conjugates were purified through gel filtration with a Sephadex G-25 column.

MR imaging procedure: MR imaging was performed with a 9.4 T MRI instrument with a micro-47 surface coil (Bruker Analytische GmbH, DSX 400 MHz). For T2*-weighted MR gradient echo imaging, the following parameters were adopted: point resolution of 117 × 117 μm², section thickness of 0.4 mm, TR = 500 ms, TE = 5 ms, number of acquisitions = 4, flip angle = 30°.

Received: July 28, 2006

Published online: November 14, 2006

Keywords: colloids · diagnostic agents · hybrid materials · nanotechnology · NMR imaging

- [1] a) A. P. Alivisatos, *Nat. Biotechnol.* **2004**, *22*, 47–52; b) R. Elgahanian, J. J. Storhoff, R. C. Mucic, R. L. Lestinger, C. A. Mirkin, *Science* **1997**, *277*, 1078–1081; c) X. Michalet, F. F. Pinaud, L. A. Bentolila, J. M. Tsay, S. Doose, J. J. Li, G. Sundaresan, A. M. Wu, S. S. Gambhir, S. Weiss, *Science* **2005**, *307*, 538–544.
- [2] a) H. Ow, D. R. Larson, M. Srivastava, B. A. Baird, W. W. Webb, U. Wiesner, *Nano Lett.* **2005**, *5*, 113–117; b) X. Zhao, R. Tapecc-Dytioco, W. Tan, *J. Am. Chem. Soc.* **2003**, *125*, 11474–11475; c) X. Zhao, L. R. Hilliard, S. J. Menchery, Y. Wang, R. P. Bagwe, S. Jin, W. Tan, *Proc. Natl. Acad. Sci. USA* **2004**, *101*, 15027–15032; d) T. J. Brunner, P. Wick, P. Manser, P. Spohn, R. N. Grass, L. K. Limbach, A. Bruinink, W. J. Stark, *Environ. Sci. Technol.* **2006**, *40*, 4374–4381; e) D. J. Bharali, I. Klejbor, E. K. Stachowiak, P. Dutta, I. Roy, N. Kaur, E. J. Bergey, P. N. Prasad, M. K. Stachowiak, *Proc. Natl. Acad. Sci. USA* **2005**, *102*, 11539–11544.
- [3] a) L. Josephson, C. H. Tung, A. Moore, R. Weissleder, *Bioconjugate Chem.* **1999**, *10*, 186–191; b) M. Zhao, D. A. Beauregard, L. Loizou, B. Davletov, K. M. Brindle, *Nat. Med.* **2001**, *7*, 1241–1244; c) D. Artemov, N. Mori, B. Okolie, A. M. Bhujwala, *Magn. Reson. Med.* **2003**, *49*, 403–408; d) R. Weissleder, A. Moore, U. Mahmood, R. Borade, H. Benveniste, E. A. Chiocca, J. P. Basilion, *Nat. Med.* **2000**, *6*, 351–355.
- [4] a) O. Veiseh, C. Sun, J. Gunn, N. Kohler, P. Gabikian, D. Lee, N. Bhattarai, R. Ellenbogen, R. Sze, A. Lallahan, J. Olson, M. Zhang, *Nano Lett.* **2005**, *5*, 1003–1008; b) M. F. Kircher, U. Mahmood, R. S. King, R. Weissleder, L. Josephson, *Cancer Res.* **2003**, *63*, 8122–8125; c) E. A. Schellenberger, D. Sosnovik, R. Weissleder, L. Josephson, *Bioconjugate Chem.* **2004**, *15*, 1062–1067.
- [5] a) R. Probstmeier, A. Bilz, J. Schneider-Schaulies, *J. Neurosci. Res.* **1994**, *37*, 324–335; b) U. Rutishauser, M. Watanabe, J. Silver, F. A. Troy, E. R. Vimr, *J. Cell Biol.* **1985**, *101*, 1842–1849; c) M. Fukuda, *Cancer Res.* **1996**, *56*, 2237–2244; d) U. Rutishauser, *J. Cell. Biochem.* **1998**, *70*, 304–312.
- [6] a) R. Seidenfaden, A. Krauter, F. Schertzinger, R. Gerardy-Schahn, H. Hildebrandt, *Mol. Cell. Biol.* **2003**, *23*, 5908–5918; b) D. Figarella-Branger, P. Durbec, G. N. Rougon, *Cancer Res.* **1990**, *50*, 6364–6370; c) L. Daniel, P. Durbec, E. Gautherot, E. Rouvier, G. Rougon, D. Figarella-Branger, *Oncogene* **2001**, *20*, 997–1004.
- [7] a) Y. Jun, Y.-M. Huh, J.-s. Choi, J.-H. Lee, H.-T. Song, S. J. Kim, S. Yoon, K.-S. Kim, J.-S. Shin, J.-S. Suh, J. Cheon, *J. Am. Chem. Soc.* **2005**, *127*, 5732–5733; b) Y.-M. Huh, Y. Jun, H. T. Song, S. Kim, J.-s. Choi, J.-H. Lee, S. Yoon, K.-S. Kim, J.-S. Shin, J.-S. Suh, J. Cheon, *J. Am. Chem. Soc.* **2005**, *127*, 12387–12391.
- [8] a) J. M. Perez, L. Josephson, T. O’Loughlin, D. Hogemann, R. Weissleder, *Nat. Biotechnol.* **2002**, *20*, 816–820; b) J.-F. Berret, N. Schonbeck, F. Gazeau, D. El Kharrat, O. Sandre, A. Vacher, M. Airiau, *J. Am. Chem. Soc.* **2006**, *128*, 1755–1761.
- [9] J.-S. Shin, J. S. Lin, P. W. Anderson, R. A. Insel, M. H. Nahm, *Infect. Immun.* **2001**, *69*, 3335–3342.